13th International Symposium on Particle Image Velocimetry – ISPIV 2019
Munich, Germany, July 22-24, 2019

PIV investigation of the flow around a superhydrophobic obstacle

Gaetano Maria Di Cicca[1]*, Gaetano Iuso[1], Michele Onorato[2]

[1]Dipartimento di Ingegneria Meccanica e Aerospaziale, Politecnico di Torino, Italy

[2]Accademia delle Scienze di Torino, Turin, Italy

*gaetano.dicicca@polito.it

Abstract

The flow around a semi-cylindrical two-dimensional obstacle is studied using Particle Image Velocimetry, comparing the case of a superhydrophobic surface with the case of a smooth surface. Measurements were carried out in a closed-loop water tunnel for a relatively low Reynolds number. Results show that the von Karman type vortex shedding observed in the canonical case is almost suppressed in the superhydrophobic case. As consequence of this suppression the whole flow field around the obstacle shows a much less unsteady behavior. It is argued that the shedding suppression is a consequence of the fact that the superhydrophobic surface avoids a critical accumulation of surface vorticity around the body due to modified slip conditions.

1 Introduction

The characteristics of the flow around a cylindrical structure in proximity of the wall or partially buried has been the subject of many numerical and experimental studies. The main interests of these studies were related to the investigation of the hydro-dynamic loads, the positions of the separation points on the cylinder surface, the lengths of the upstream and downstream separation regions, the vortex shedding mechanisms and the scour and self-burial process. The effects of the gap ratio G/D (G is the distance between the bottom wall and the downward surface of the cylinder and D is the diameter of the cylinder), the burial ratio B/D (B is the burial depth), the Reynolds number and the ratio δ/D (δ is the boundary layer thickness) were deeply analysed. An extensive bibliography on the subject can be found in Akoz (2012).

In the present paper the flow around a partially buried circular cylinder (B/D=0.5) on a smooth plane boundary is studied, for a relatively low Reynolds number, using Particle Image Velocimetry. The case in which the obstacle is coated with a random-textured superhydrophobic surface is compared with the case of a smooth surface. The present research is related to the understanding of the role of slip conditions in presence of pressure gradients (see e.g. You and Moin, 2007; Huang *et al.*, 2018) in order to provide useful information for flow control strategy.

2 Experimental setup and flow conditions

In Fig. 1a the sketch of the semi-cylindrical two-dimensional obstacle is shown. The cylinder axis is perpendicular to the incoming flow. The burial ratio B/D is equal to 0.5 . The ratio between the span of the obstacle and its diameter is equal to 11.7 .

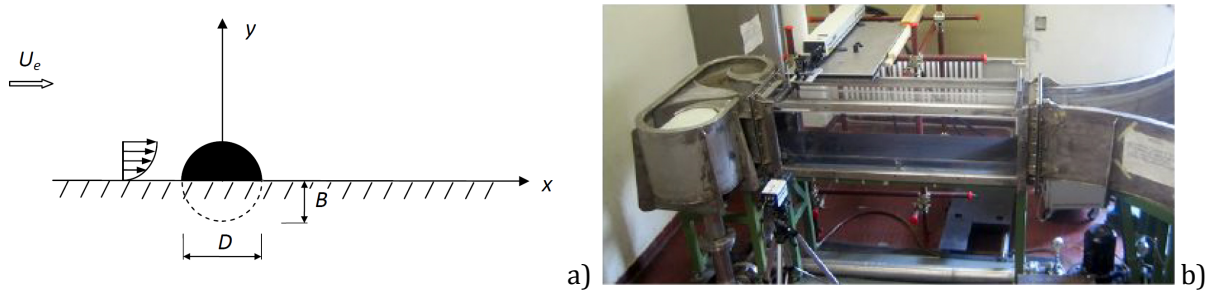

Figure 1: a) Sketch of the semi-cylindrical two-dimensional obstacle; b) "Hydra" water tunnel.

In the superhydrophobic case the surface was prepared by using a double layer spray coating method (NeverWet® superhydrophobic coating). An extreme contact angle of about 165° and a hysteresis contact angle of about 4° were evaluated. The experiments were carried out in the water tunnel at the "Dipartimento di Ingegneria Meccanica e Aerospaziale" of the Politecnico di Torino. This facility is a closed-loop open-surface channel with a 350 mm wide, 500 mm high, and 1800 mm long test section (Fig. 1b).

Both for the canonical case and for the superhydrophobic case the Reynolds number, based on the cylinder diameter and on the incoming flow velocity U_e , is about 360. The incoming boundary layer is laminar and the boundary layer thickness, in absence of the obstacle, is about equal to the obstacle height. The PIV system consisted of a 1280x1024 pixels high speed NanoSense MKIII CMOS camera and a continuous Spectra-Physics argon laser, with a maximum emitted power of 6 W. The laser beam was expanded by a cylindrical lens and focused by a spherical lens, forming a light sheet with a thickness of about 0.5 mm. The water was seeded with spherical hollow glass particles, 10 microns nominal diameter, which were small enough to follow the flow. PIV measurements were taken in the streamwise wall-normal plane (x,y). The physical size of the PIV images was 64.5x60mm^2 (2.15D x 2D). The PIV analysis was done with the "LaVision DAVIS 7.2" software to perform the correlations to obtain the velocity fields. The local particle displacements were determined using an adaptive cross-correlation algorithm. The final interrogation window size was 32x32 pixels, overlap of 50%. The obtained vectors were validated using a minimum peak height in the correlation, which was 1.2 times the height of the second highest peak. Erroneous vectors were substituted applying a moving average filter with a kernel of 5x5 vectors. Each velocity vector is representative of the mean velocity in an area of 1.7x1.7mm^2 (0.06Dx0.06D).

3 Results and comments

The maps of the longitudinal (U) and vertical (V) component of the mean velocity are shown in Fig. 3 and Fig. 4 respectively. On both figures the time-averaged streamlines are also represented.

Although the mean flow structure does not appear greatly influenced by the different slip conditions, a wider (and presumably longer) wake can be observed in the superhydrophobic case.

Similar flow behaviour was also observed for isolated circular cylinders coated with superhydrophobic surfaces (Muralidhar *et al.*, 2011).

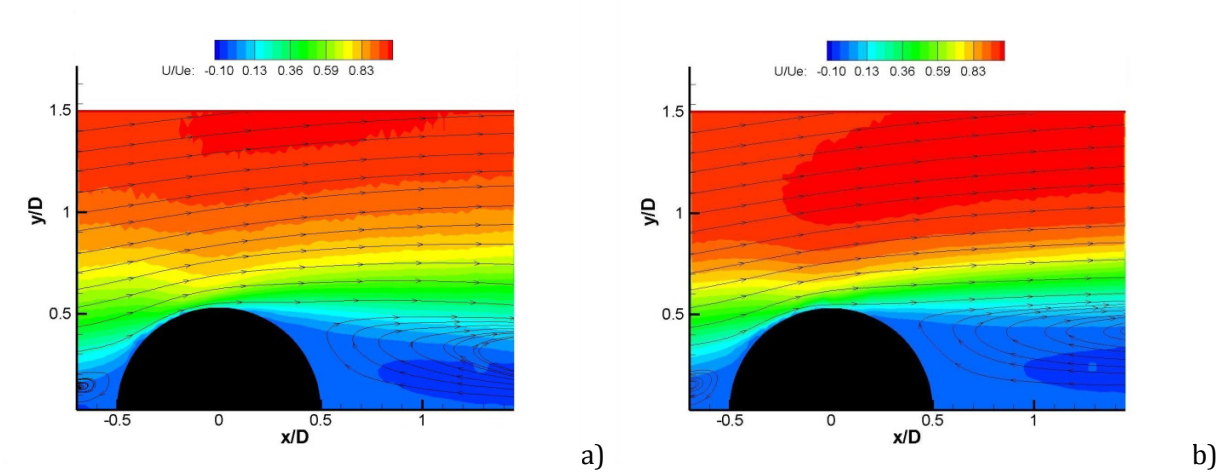

Figure 3: Longitudinal component of the mean velocity and time-averaged streamlines.
a) Smooth surface; b) Superhydrophobic surface.

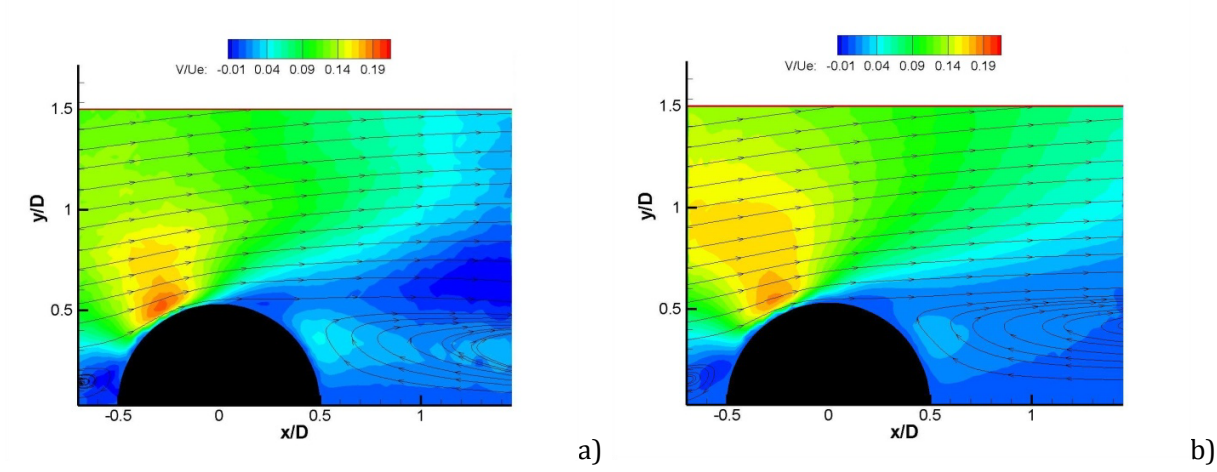

Figure 4: Vertical component of the mean velocity and time-averaged streamlines.
a) Smooth surface; b) Superhydrophobic surface.

The maps of the RMS of the longitudinal component of the fluctuating velocity are shown in Fig. 5. A much less unsteady flow configuration is observable in the case of the superhydrophobic surface. Also, in the regions of the obstacle leading edge and trailing edge more stable clockwise vortical structures are present. The band of high fluctuation throughout the whole domain, observed in the case of the obstacle with a smooth surface, is absent in superhydrophobic case.

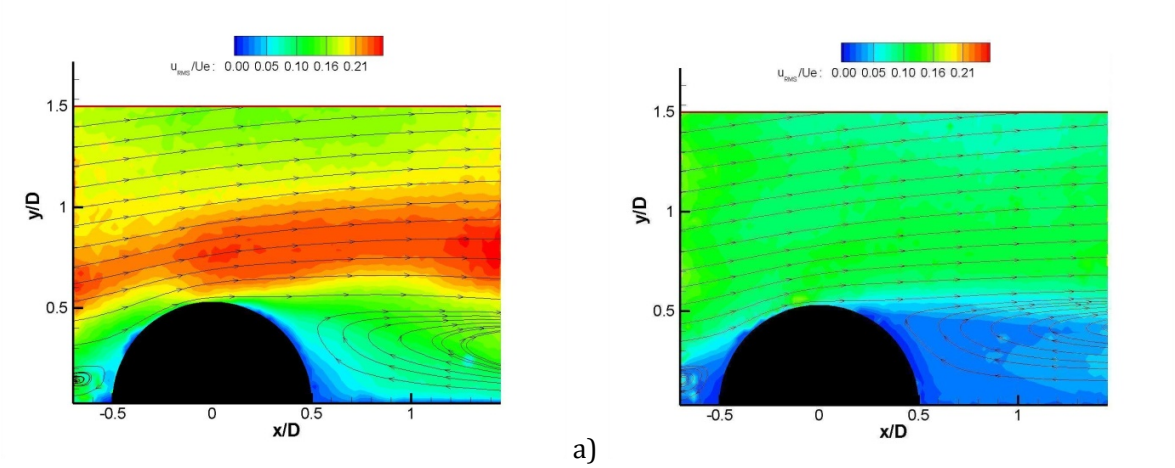

Figure 5: RMS of the longitudinal component of the fluctuating velocity and time-averaged streamlines. a) Smooth surface; b) Superhydrophobic surface

In Fig. 6 the maps of the probability for the flow to have positive longitudinal instantaneous velocity (forward flow probability, FFP) are reported. Also from this representation of the flow it is clearly evident that the superhydrophobic obstacle possesses a much less unsteady wake. In the superhydrophobic case an extended region of the separated flow is characterized by FFP values almost close to zero while values close to 0.5 are observable in a large part of the wake of the canonical case.

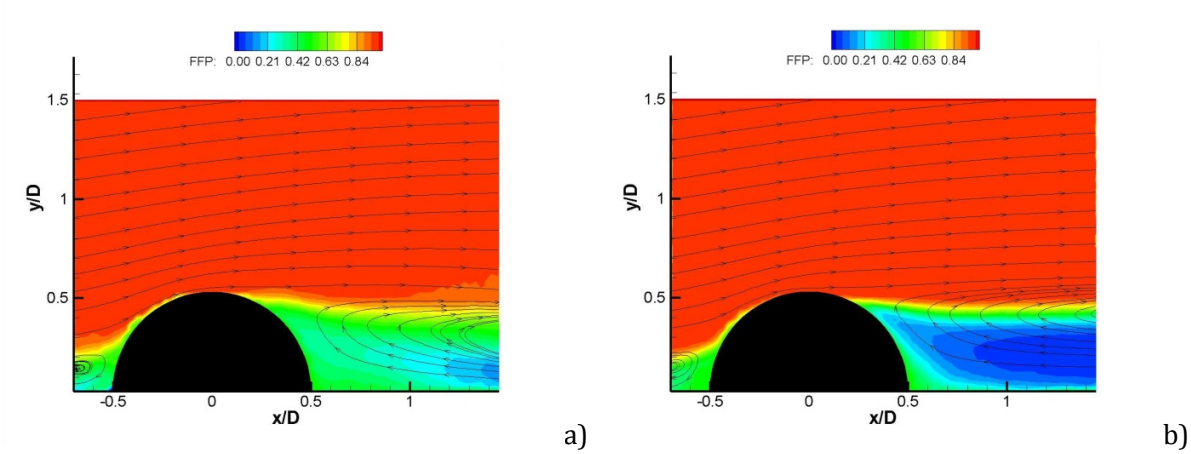

Figure 6: forward flow probability (FFP) and time-averaged streamlines.
a) Smooth surface; b) Superhydrophobic surface.

The much less unsteady flow configuration in the wake of the obstacle for the superhydrophobic case (Figs. 5b and 6b) is also confirmed by the spectra shown in Fig. 7, where the amplitude is normalized with respect to the peak amplitude corresponding to the canonical case. The Strouhal number (St) is based on the cylinder diameter and on the flow velocity U_e . The spectra refer to the vertical component of the velocity and were computed in the wake shear layer at $x/D \cong 0.52$ and $y/D \cong 0.45$. While the canonical case shows a strong peak at St equal to about 0.27, indicating a von

Karman type vortex shedding from the obstacle surface, this shedding appears to be almost suppressed as a consequence of the slip conditions present in the superhydrophobic case.

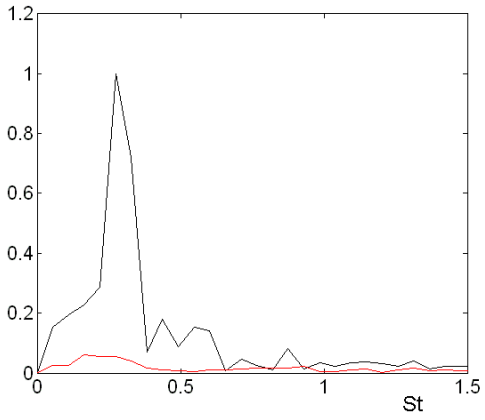

Figure 7: Relative amplitude spectra in function of the Strouhal number.
Black line: canonical case. Red line: superhydrofobic case.

Similarly to what was observed in related studies on wake instability of axisymmetric bodies (Leal 1989), it is argued that the vortex shedding arises when the surface vorticity accumulated around the obstacle surface exceeds some critical value. Consequently, it is conjectured that, due to modified slip conditions, the superhydrophobic coating is able to avoid the critical accumulation of surface vorticity around the body thus leading to the vortex shedding suppression. However, further investigations are necessary for a deeper understanding of this shedding suppression mechanism.
In order to capture the essential flow dynamics in the two investigated cases, a proper orthogonal decomposition (POD) analysis was performed. In Fig. 8 an example of the reconstructed snapshots using the first three POD modes are shown. The instantaneous velocity field is superimposed to the colour map representing the spanwise vorticity. High values of positive and negative vorticity are visualised with red and blue colors respectively. In both cases over the upper surface of the obstacle high positive values of the vorticity are observable. High negative values of the vorticity are observed over the rear surface of the buried cylinder when a vortical structure is shed (Fig. 8a). Analysing the time series of the reconstructed signal for the superhydrophobic case (see for instance Fig. 8b), the almost complete absence of vortical structures shed from the obstacle is observable.

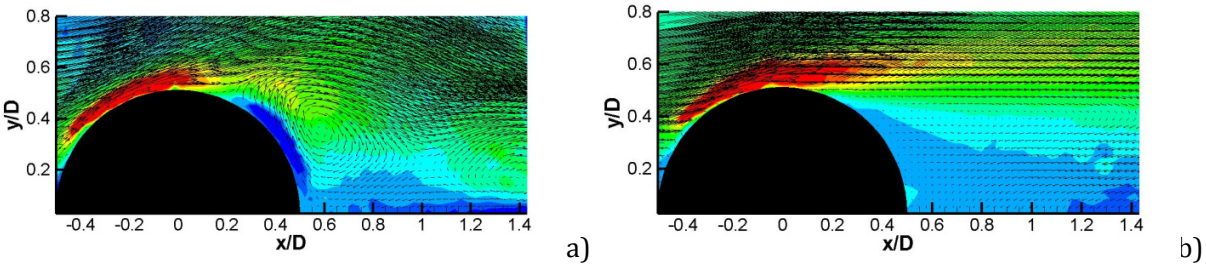

Figure 8: POD reconstructed snapshots. The instantaneous velocity field is superimposed to the colour map representing the spanwise vorticity. a) Smooth surface; b) Superhydrophobic surface.

4 Conclusion

PIV measurements at a Reynolds number equal to 360 of the flow around a superhydrophobic semi-cylindrical obstacle have been shown in comparison with the flow around the uncoated obstacle. The maps of the longitudinal and vertical component of the mean velocity show that, although the mean flow structure does not appear greatly influenced by the different slip conditions, a wider wake can be observed in the superhydrophobic case.
The maps of the RMS of the longitudinal component of the fluctuating velocity and the maps of the forward flow probability (FFP) show that the flow around the superhydrophobic obstacle is characterized by a much less unsteady behaviour.
The spectra of the vertical component of the velocity in the wake shear layer show that the von Karman type vortex shedding observed in the canonical case is almost suppressed in the superhydrophobic case. It is argued that the shedding suppression is a consequence of the fact that the superhydrophobic surface avoids a critical accumulation of surface vorticity around the body due to modified slip conditions. The reconstructed snapshots from the POD analysis contributes to reveal the essential flow dynamics for the two investigated cases.

References

Akoz MS (2012) Investigation of vortical flow characteristics around a partially buried circular cylinder. *Ocean Engineering*, 52, 35:51

Huang H, Liu M, Gu H, Li X, Wu X, and Sun F (2018) Effect of the slip length on the flow over a hydrophobic circular cylinder. *Fluid Dynamics Research* 50, 025515

Leal LG (1989) Vorticity transport and wake structure for bluff bodies at finite Reynolds number. *Physics of Fluids* A 1, 124:131

Muralidhar P, Ferrer N, Daniello R, and Rothstein JP (2011) Influence of slip on the flow past superhydrophobic circular cylinders. *Journal of Fluid Mechanics* 680, 459:476

You D, and Moin P (2007) Effects of hydrophobic surface on the drag and lift of a circular cylinder flows over rough walls. *Physics of Fluids* 19, 081701